Article

Bioinspired Coastal Barriers: A Preliminary Laboratory Study on the Hydraulic Performances of Shapes Inspired by Marine Organisms

Valentina Perricone [1,2], Pasquale Contestabile [1,3,*], Antonio Mele [1], Nasrin Hassanpour [1], Diego Vicinanza [1,2,3,*] and Mario Buono [1]

1   Department of Engineering, University of Campania "Luigi Vanvitelli", 81031 Aversa, Italy; valentina.perricone@unicampania.it (V.P.); antonio.mele1@unicampania.it (A.M.); nasrin.hassanpour@unicampania.it (N.H.); mario.buono@unicampania.it (M.B.)
2   Stazione Zoologica Anton Dohrn, Villa Comunale, 80121 Napoli, Italy
3   CoNISMa, National Inter-University Consortium of Marine Sciences, P.le Flaminio 9, 00196 Roma, Italy
*   Correspondence: pasquale.contestabile@unicampania.it (P.C.); diego.vicinanza@unicampania.it (D.V.)

Abstract: Coastal erosion, extreme climate events, and the loss of biodiversity are important consequences of climate change that directly impact our society. The needs to develop effective engineering practices using nature as model and mentor are now emerging aimed to develop high-performance coastal infrastructures integrating and sustaining local marine ecosystems. In this scenario, the present article describes the concept development and preliminary experimentation of simplified bioinspired models to evaluate their hydraulic performances. This study is part of a future vision to develop submerged barriers, printed with eco-friendly materials, characterized by high hydraulic performances and cable of supporting local biodiversity. Following a top-down approach, the functional features of key organisms were abstracted and transferred to create three bioinspired models. The hydraulic performance of these models is analyzed in terms of wave transmission, reflection, and dissipation under various wave conditions. Under certain circumstances, the bioinspired barriers demonstrate wave attenuation comparable to traditional submerged breakwaters. A method based on skin friction and drag-related processes provides a simple heuristic explanation of how the shape of the models affect the transmission coefficient. The results achieved offer valuable insights for the design of future coastal defense systems that are inspired by, and integrated with, natural ecosystems.

Keywords: bioinspiration; nature-based solution; coastal protection; barriers; wave transmission

1. Introduction

Climate change is occurring at a faster rate and the severe environmental consequences are well known, including sea level rise, coastal flooding and erosion, and extreme weather events [1,2]. Efficient coastal barriers are essential to provide future generations with crucial protective and regulating ecosystem services [3,4]. Since the early 20th century, particularly after World War II, the most common shore protections relied on emerged, detached rubble-mound breakwaters. Built as shore-parallel barriers in shallow waters, these structures have probably existed for approximately 3000 years with the Phoenician breakwater at Atlit in Israel dated around the 8th century BC [5]. Traditional breakwaters have effectively mitigated storm waves, maintaining high structural integrity over time [6]. As implied by the term "breakwater", these constructions were designed as majestic constructions, generally oversized, forcing larger waves to break and thus reducing the incident wave energy [7]. Nonetheless, some undesirable environmental consequences have been observed, such as water anoxia, unintended nearshore currents, and land/seascape degradation [8–10]. To mitigate these impacts, engineers began to employ alternative solutions in the early 1980s, i.e., low-crested structures, commonly known as submerged breakwaters (SBs) [11]. Albeit

the ecological effects of SBs were not fully recognized, there was a perception that they were a more environmentally friendly option. This assumption was not critically examined until 2013, when further research began to address the environmental issues associated with coastal defenses. In this context, two European projects, THESEUS [12] and DELOS [13], played a critical role in supporting the development of cost-effective and more sustainable coastal structures. Recent comprehensive analyses on breakwaters have highlighted multiple concerns about SBs, suggesting that all these kinds of "hard or grey solutions" may become unsustainable in the near future due to their adverse effects on local and adjacent coastal geomorphology and biodiversity [3,10,14,15]. Albeit SBs provide protection without visual impacts, their hydro-morphodynamic behavior is more complex [16,17]. They act as "wave terminators", absorbing energy mostly in the direction of the incoming waves, but, at the same time, sediment transport patterns are strongly altered, with no possibility for sediments to pass from offshore to inshore (and vice versa); as result, in certain conditions, submerged structures contributed in various ways to shoreline erosion [18]. A possible solution could be the use of more permeable SBs (e.g., [19]), and the bioinspired coastal defense proposed in this work advances towards this approach. However, no definitive conclusions can be suggested about the relationship between permeability and sediment transport due to the lack of knowledge on the underlying processes. However, a rapid transition from gray to green infrastructures and approaches are now emerging [20].

Recent approaches entail the development of coastal barriers that are able to dissipate wave action and reduce erosion while minimizing environmental impacts and including coherent physical conditions that support local biodiversity, such as permeability and habitat-forming features [3,10,14]. Noteworthy are the so-called nature-based solutions (NbSs), which utilize natural habitats, such as coral reefs, seagrasses, or mangroves, to mitigate hazards while simultaneously promoting local biodiversity [21–24]. They involve actions aimed at implanting, safeguarding, managing, and/or restoring natural ecosystems that provide essential coastal and ecosystem services for both human well-being and biocenosis [21–24]. Numerous studies have been recently reported in the literature regarding the effectiveness of natural habitats, NbSs, and related approaches on coastal protection (see the review provided by Perricone et al. [10] and references therein).

Nonetheless, NbSs have limitations, including the need for larger spaces, specific suitable conditions, extended time frames for full establishment and development, high sensibility from anthropogenic impacts, seasonal variations, and interactions with adjacent ecosystems [21,22,25,26]. Hence, for immediate coastal protection, hybrid measures incorporating artificial scaffolds are often necessary for habitat implantation and may still be insufficient in highly turbulent and exposed areas, which necessitate fully artificial barriers. In response to these challenges, bioinspired strategies are developing, in which nature is used as a model and mentor to realize high-performance bioinspired barriers for coastal protection, which can effectively support biological installation and/or substitute the habitat creating a new barrier [10,27]. The bioinspired approach entails the identification of key functionalities and essential working principles that underpins biological systems to inform design and solve technical problems. Recently, there has been a surge in the development of 3D-printed artificial reefs, some of which are also bioinspired [28]. Some of the most fascinating examples in this field are the Modular Artificial Reef Structure (MARS) created by Reef Design Lab [29] and the 3DPARE modules used for coral restoration [30]. Notable is the study by Stachew, Houette, and Gruber [27], including a mangrove root-inspired design for coastal protection and showcasing the bioinspired process from biological study to conceptual technical design. By thoroughly examining mangrove root morphology, the researchers abstracted strategies such as adaptive soil penetration, surface texture, complex topology, hierarchical morphology, self-healing materials, and growth principles. These strategies were then translated into several conceptual designs for multifunctional foundations and infrastructures. The resulting designs effectively anchor structures, prevent erosion, adapt to various stresses, and create habitats for living organisms.

In this framework, the present article describes the concept development and preliminary experimentation of simplified bioinspired models evaluating their hydraulic performances. This work is part of a broader vision to develop a "submerged forest", where bioinspired and biobased barriers effectively integrate with and promote the local ecosystem. The main question that this work aims to address regards the identification of bioinspired shapes that can effectively attenuate wave actions.

Following a top-down approach, technical problems and opportunities were identified, and functional features of key organisms were abstracted, simplified, and transferred to create bioinspired models aimed at enhancing hydraulic performance, ensuring permeability and subsequently integrating in the future with local biodiversity.

Three bioinspired models were generated evaluating their hydraulic performances in terms of wave transmission, reflection, and dissipation under various wave conditions. Accordingly, the article is organized as follows: Section 2 describes the design inspiration and implementation of the three coastal barrier models; Section 3 presents the experimental setup, wave conditions, and methodology; Section 4 reports the experimental results; Section 5 provides a discussion of the results and some additional considerations; and, finally, key findings and conclusions are drawn in Section 6.

2. Design Inspiration and Implementation

The design concept of bioinspired breakwaters was developed based on a top-down design strategy starting from the identification of problems and opportunities that a new design should address, followed by the research of analogous functions and contexts in nature until the abstraction and transfer of biological strategies to the final design.

The definition of the problem started from the analysis of the context, specifically the coastline and related infrastructures. Numerous artificial infrastructures have been realized to protect coastlines against destructive wave and wind forces. Traditional infrastructures consist of hard engineering solutions, such as seawalls, jetties, and breakwaters, and rock groynes are considered to be unsustainable in the near future since they are: (1) bulky and monofunctional, occupying a vast space and absolving the only coastal defense role; (2) homogeneous, supporting low biodiversity and non-native species proliferation; and (3) unadaptable, necessitating continuous maintenance or rebuilding over time [31,32].

Hence, the arising question was: how does nature stabilize and protect coastlines while promoting local biodiversity? The answer can be found in some marine ecosystems, such as coral reefs, oyster reefs, mangroves, salt marshes, and seagrasses that act as a natural defense for the coastlines [10]. Indeed, these ecosystems are able to function as a barrier, particularly through massive wave reduction and sediment stabilization, while also providing additional ecosystem services, such as climate regulation, CO_2 absorption, and biological control [14,33]. Among them, seagrasses are one of the main habitats that have been studied for their numerous ecosystem services and key characteristics of coastal protection. Seagrasses are marine flowering plants evolved from terrestrial ones that colonized the submerged photic zone about 70 MA ago. They are firmly anchored to sediment by a high-density matrix of roots and rhizomes. *Posidonia oceanica* is the endemic species of the Mediterranean Sea, which forms wide underwater meadows. Seagrass meadows/beds play a key role in facilitating settlement and refuge as well as slowing the water movement and reducing wave energy. Particularly, the hydrodynamic effects of seagrass beds on wave attenuation, current flow, and sediment dynamic have been widely studied and described (see [10,34] and the literature cited therein). Key functional strategies have been selected here from seagrasses based on their influence on wave motion, current flow, and sediment dynamics. Submerged seagrass beds are able to reduce the speed of currents and dissipate wave energy through the deflation of water flow and friction effects within plants, where longitudinal advection effects and turbulence are generated. The density, biomass, submergence ratio (plant height/water depth), and rigidity of seagrass leaves can influence the hydrodynamic effects [34,35]. Wave and current attenuation depend on density and biomass that are related to the number of shoots per unit area as

well as the number and size of leaves [34–37]. Seagrasses that occupy a higher proportion of the water column have more success in reducing waves and currents [38,39]. John et al. [40] demonstrated that very important parameters affecting the wave transmission coefficient are the relative plant height, the meadow parameter, and the relative meadow width. For a wider seagrass meadow, the percentage reduction in wave run-up rises by 41%.

Starting from a bioinspiration and simplification of seagrass morphology, three models were generated (Figure 1). The first bioinspired model (L-Type) was designed as a basic leaf-shaped system. From this model, a second model (T-Type) was successively implemented, characterized by its triangular shape to further deviate the flow and increase force impact resistance. The shape emerged as a simplified abstraction from aquatic animals, which possess a number of morphological and behavioral adaptations to resist or move in fluids. In particular, the streamline shape is a well-known convergent design present in multiple phylogenetically distant species able to reduce resistive drag and modify water flow over the body [41]. Additionally, some marine organisms that need to deviate the flow and dive (i.e., jump out of and re-enter the water) have elongated bilateral shapes, such as fishes, dolphins, and others. Their shape can resist extreme impact force, especially as they re-enter the water at high speeds [42]. An additional version of this model was developed, model HT-Type, characterized by the addition of a circular head at the top to increase the visibility at the surface as a buoy, providing future navigation and weather data as well as increase the buoyancy of the structure.
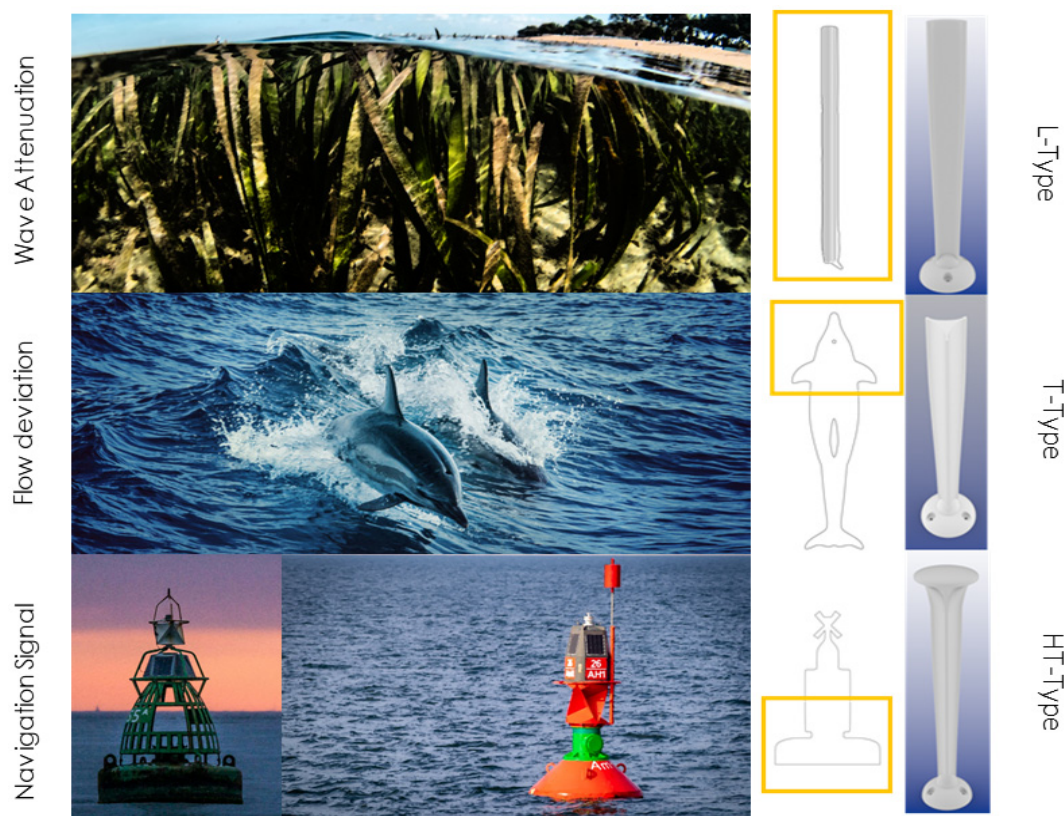

Figure 1. Design inspirations and related models. The yellow boxes indicate the identified functional shapes.

The three models were subsequently prototyped in scale and hydrodynamically analyzed, comparing them to a cylinder-shaped model (C-Type) used as the control.

3. Experimental Setup and Data Analysis

3.1. Model Prototyping

The L-Type, T-Type, HT-Type, and C-Type models were generated in 3D CAD using Rhinoceros (version 7, released in 2020) and printed in a 1:25 length scale (Froude scaling), with respect to the expected final-sized barriers. Figure 2 and Table 1 provide the technical drawing with the geometrical characteristics and related dimensions of the tested models. The models were printed at 245° using an Anycubic Chiron 3D printer based on FDM technology and setup on a layer height of 0.20 mm, infill of 20%, and speed of 50 mm/s. The material used was polyethylene terephthalate glycol, which was chosen because it is recyclable and has desirable physical–chemical characteristics: hardness, impact and chemical resistance, ductility, ease of extrusion, and good thermal stability.
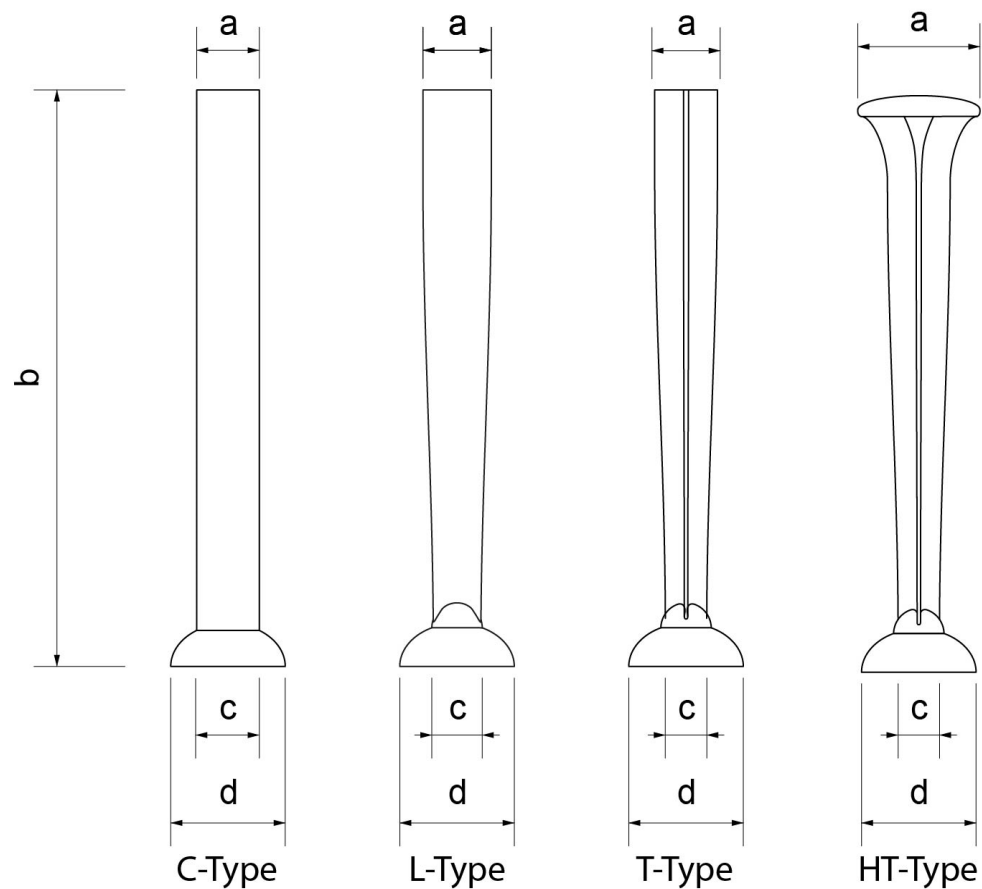

Figure 2. Model prototypes: technical drawing including definition of (a) upper width, (b) height, (c) lower width and (d) diameter of the base. Related dimensions are referenced in Table 1.

Table 1. Main geometrical parameters for tested models. Measures are in mm.

	a	b	c	d
C-Type	27	250	27	50
L-Type	30	250	20	50
T-Type	27	250	18	50
HT-Type	53	250	18	50

3.2. Key Hydraulic Parameters, Instrumentation, and Model Setup

To assess the total wave disturbance provided by the transmitted wave, the printed prototype models were tested at the Maritime Engineering Laboratory at the University of Campania "L. Vanvitelli" (Italy). The wave flume had a length of 13.4 m, a width of

0.8 m, and a depth of 0.6 m (Figures 3 and 4). The bottom of the model was non-erodible. Moving away from the wave generator, it was flat for about 3 m and then gradually sloped to a 1:22 slope. Controlled wave generation is achieved by a piston-type wave paddle, particularly suited for intermediate depth waves. The software AwaSys (version 5, Aalborg University, 2010) was used to generate waves with a simultaneously active absorption of reflected waves. In addition, a dissipative gravel beach was placed at the far end of the flume to absorb the final transmitted wave energy and minimize reflections in the flume. The control software allowed the generation of regular and irregular waves.
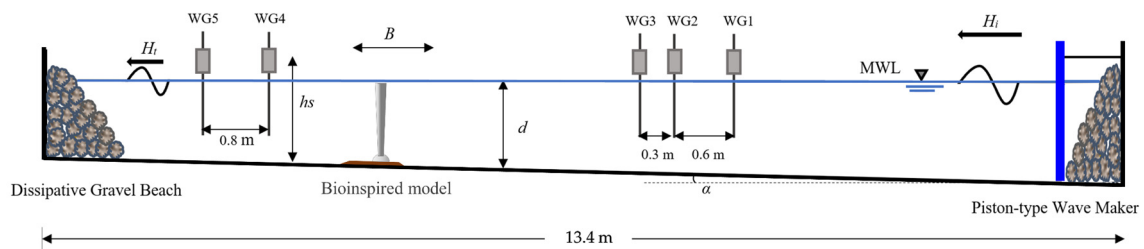

Figure 3. Schematic view of the wave flume and experimental equipment.

Figure 4. View of the laboratory arrangement and model setup.

To separate incident and reflected waves, three wave gauges were installed near the model, based on suggestions by Klopman and van der Meer [43]. The incident and reflected spectra were determined using the approach of Mansard and Funke [44]. Wave transmission was evaluated by means of two wave gauges placed on the rear sides of the models. The sampling frequency of all wave gauges was set to 30 Hz. The concluding section of the wave flume, specifically the part constituting a dissipative gravel beach, was intentionally left open on the sides. Since the waves were also propagated outside the wave flume as part of the whole wave basin, more realistic water circulation at the rear of the structure was ensured, preventing the occurrence of an artificial wave setup behind the breakwater.

The printed models (16 for each type) were mounted on a perforated metal board in a straight horizontal line configuration. The metal board was 439 mm wide with a length of 800 mm and height of 20 mm. T-Type and HT-Type models having a triangular shape were also tested in a 180° rotated configuration, where the base of the triangle was directed toward the wave front (respectively, designated as rT-type and rHT-Type). Hence, a total of six configurations were tested, where Figure 5 shows the model distribution for the configurations.
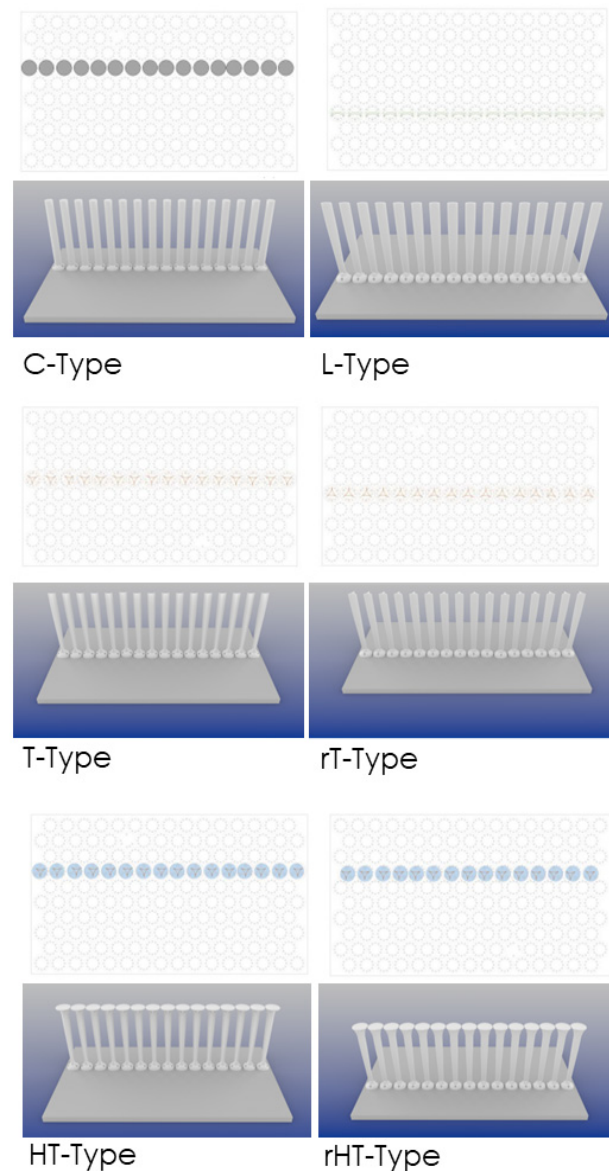

Figure 5. Schematic view of the model distribution in the six configurations.

3.3. Wave Conditions

The wave conditions were categorized into four distinct categories: regular "poor" (H_i (m) < 0.06), regular "mild" (0.07 < H_i (m) < 0.14), regular "extreme" 0.15 < H_i (m) < 0.2, and irregular "storm" waves (where $H_i = 0.14$ (m) and with peak periods equal to 0.8, 1.2, and 1.6 (s)). Irregular wave trains were generated based on the three parameters of the JONSWAP spectrum by using a peak enhancement factor, $\gamma = 3.3$, in all tests.

Each category signifies a distinct spectrum of wave climate and energy. Regular waves enhance the ability to discern interactions with wave structures, whereas irregular wave conditions enable a comprehensive evaluation of breakwater system performance and the derivation of spectral and statistical response characteristics. "Poor" regimes denote calm sea states, while "extreme" corresponds to the most elevated, non-breaking (offshore) wave conditions. Irregular "storm" waves epitomize the most intricate and demanding conditions, replicating the authentic, unprocessed time series of random waves. Graphs were generated based on these four categories to visually illustrate the variations in the transmission coefficient under different conditions. Hydrodynamic parameters are plotted against the relative deep-water wave steepness (s) (i.e., the ratio of wave height to wavelength and often used as an indicator of wave stability), calculated considering the wavenumber, K (Equation (1)), i.e.:

$$K_0 = \frac{2\pi}{L_0} \tag{1}$$

where L_0 is the deep-water wavelength.

Tables 2 and 3 report the main characteristics of simulated sea states.

Table 2. Main characteristics of regular wave conditions.

Regular "Poor"			Regular "Mild"			Regular "Extreme"		
H [m]	**T** [s]	**s** [-]	**H** [m]	**T** [s]	**s** [-]	**H** [m]	**T** [s]	**s** [-]
0.02	0.8	0.02	0.07	1.4	0.02	0.15	2	0.02
0.04	1	0.03	0.1	1.6	0.03	0.15	1.4	0.05
0.05	1.2	0.02	0.12	1.8	0.02	0.19	1.6	0.05
0.05	0.8	0.05	0.07	1	0.04	0.2	1.4	0.07
0.06	0.8	0.06	0.11	1.2	0.05	0.19	1.8	0.04
			0.1	1	0.06	0.19	2	0.03
			0.14	1.2	0.06	0.2	1.8	0.04
						0.2	2	0.03

Table 3. Main characteristics of irregular wave conditions.

Irregular "Storm"		
H$_{m0}$ [m]	**T$_{p0,2}$** [s]	**s$_p$** [-]
0.07	0.8	0.07
0.1	1.2	0.04
0.1	1.6	0.03

3.4. Performance Analysis

In coastal engineering, one of the prime concerns in studying beach defenses is the transmission coefficient, K_t, which represents the ratio of transmitted significant wave height ($H_{m0,t}$) to incident significant wave height ($H_{m0,i}$) (Equation (2)). The limits of wave transmission are defined by $K_t = 0$ (no transmission) and $K_t = 1$ (no reduction in wave height). The effectiveness of coastal structure design in mitigating wave energy and safeguarding coastal regions is crucially assessed through this coefficient.

$$K_t = \frac{H_{m0,t}}{H_{m0,i}} \tag{2}$$

Additionally, the efficiency of a submerged coastal structure requires the consideration of wave reflection and dissipation coefficients [45]. The reflection coefficient, K_r, is

determined as the ratio of reflected significant wave height ($H_{m0,r}$) to the incident one (Equation (3)).

$$K_r = \frac{H_{m0,r}}{H_{m0,i}} \tag{3}$$

Consequently, the dissipation coefficient, K_d, can be assessed by $K_d = 1 - K_r^2 - K_t^2$.

The results are reported using the wave transmission, reflection, and dissipation coefficients, assessing the hydraulic performance of the different designed models under four wave conditions: "poor", "mild", "extreme", and" storm".

4. Results

4.1. Wave Transmission

Figure 6 (upper panel) reported the K_t values for each designed model under various wave conditions. Considering the C-Type model (the cylinders) as the hydrodynamic "white", T-Type and rT-Type models showed lower values of K_t under extreme and storm waves. In particular, the T-Type model shows the lowest values of K_t for all wave climates, while the rotation of the model rT-Type determines an increase in the values, thus resulting in inferior hydraulic performances. The C-Type model presents an interesting "flat" behavior and seems to not be concerned with wave types. The addition of a "head" on the top of the T-Type model (thus obtaining the HT-Type model) determines a negative effect for K_t. By overturning the model (rHT-Type), the K_t values become even worse, with an increase of 18%, reporting the worst values.
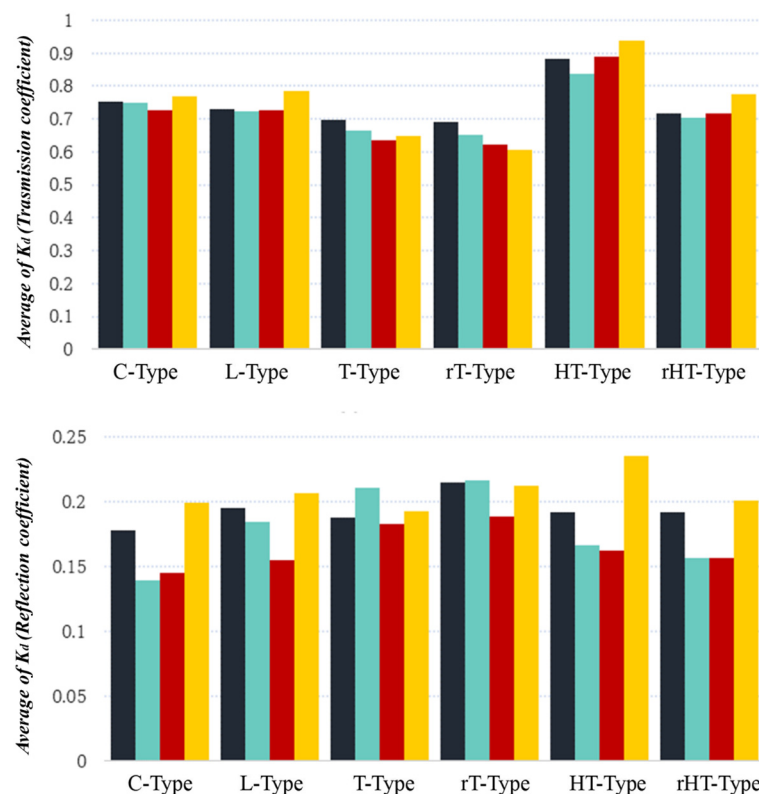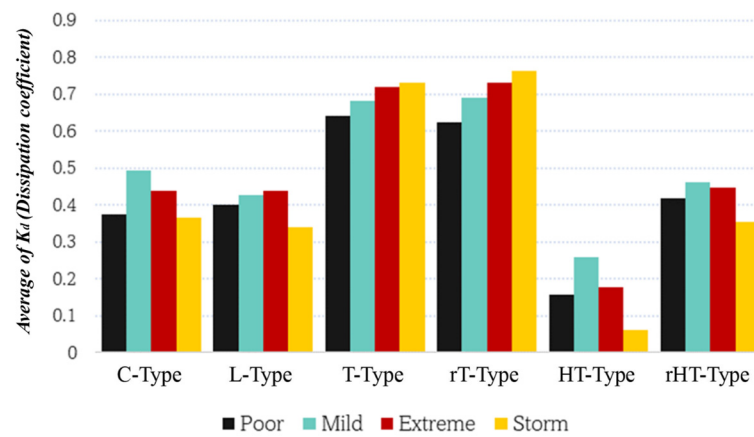

Figure 6. *Cont.*

Figure 6. Average of transmission, reflection, and dissipation coefficients in different wave climates ("poor"; "mild", "extreme", and "storm") calculated for wave transmission (**top panel**), reflection (**middle panel**), and dissipation (**lower panel**).

Hence, while the qualitative behavior of the triangular-shaped models is clear, leading to a reduction in K_t values, the quantitative effects strongly increase with the presence of the "head".

The steepness of waves significantly influences the wave transmission coefficient of coastal defense structures. Higher wave steepness suggests that the waves are steeper and more prone to breaking when they encounter a breakwater. The influence of incident wave steepness under various wave conditions is shown in Figure 7.
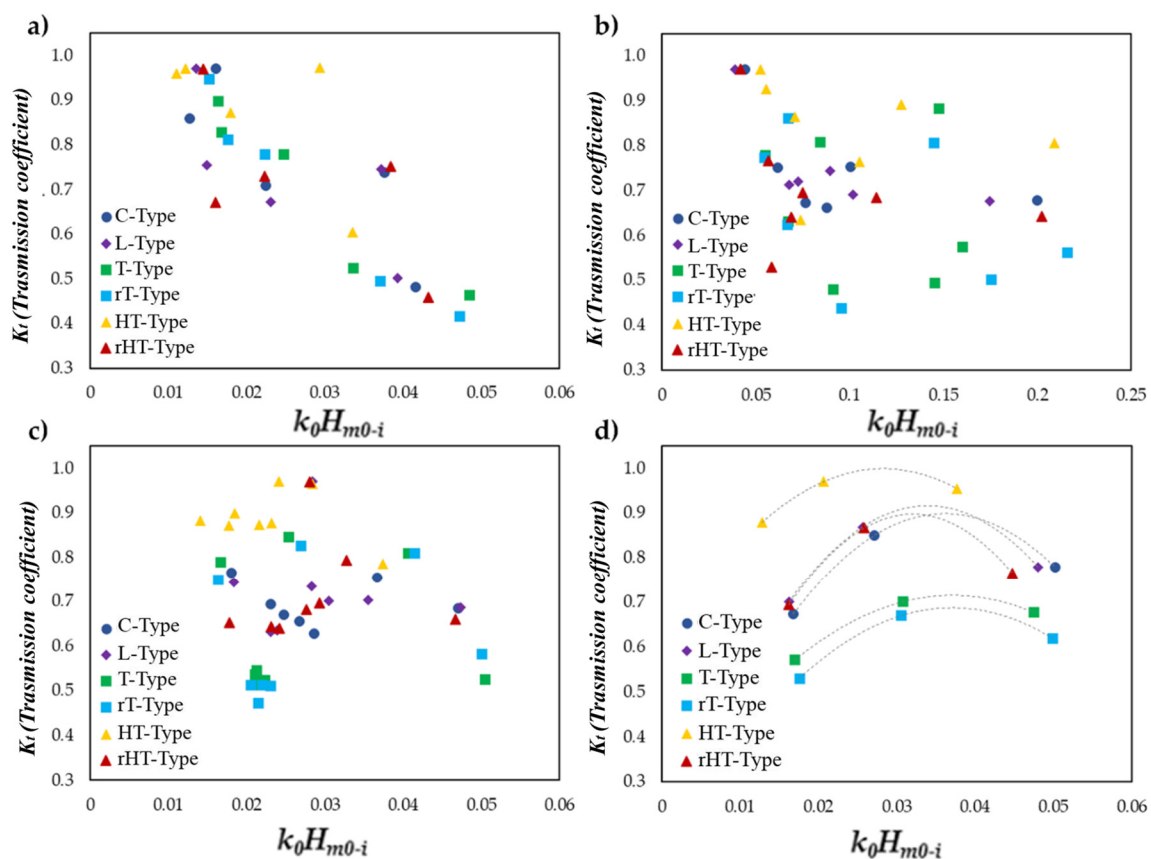

Figure 7. Transmission coefficient, K_t, versus the incident wave steepness ($k_0H_{m0\text{-}i}$) in different wave climates: (**a**) regular "poor" conditions; (**b**) regular "mild" wave conditions; (**c**) regular "extreme" wave conditions; (**d**) irregular "storm" wave conditions.

It is worth noting that the range of wave steepness for poor and extreme wave conditions is almost the same. However, with the increase in the energy level of regular waves, the non-linear effects become more evident. Random storm waves show a clearer pattern with a point of maxima for intermediate values of wave steepness. This result was almost expected, being a perception that such kinds of structures lose effectiveness under long waves (i.e., lower wave steepness).

4.2. Wave Reflection

The presence of reflected waves near the structures poses a risk to vessels navigating nearby and can limit the availability of berths within the harbor. Additionally, wave reflections can contribute to local scouring or the overall lowering of seabed levels. The tested bioinspired coastal barriers present an interesting reflection coefficient, as shown in Figure 6 (central panel). These values are often lower than the ones obtained for submerged rubble-mound breakwaters. Notably, the lowest K_r is provided by the cylindrical barrier. For all models, wave reflection under poor and mild wave climates is higher than extreme. The presence of small waves under random wave time series provides a heuristic explanation for the highest values of K_r under storm wave conditions (Figure 8). This aspect is also supported by Figure 8d, where K_r values are almost constant for all models and regardless of wave steepness. In contrast, under monochromatic wave conditions (Figure 8a), it is impossible to identify a unique pattern for wave reflection and, as for K_r, a strong non-linear effect was observed.
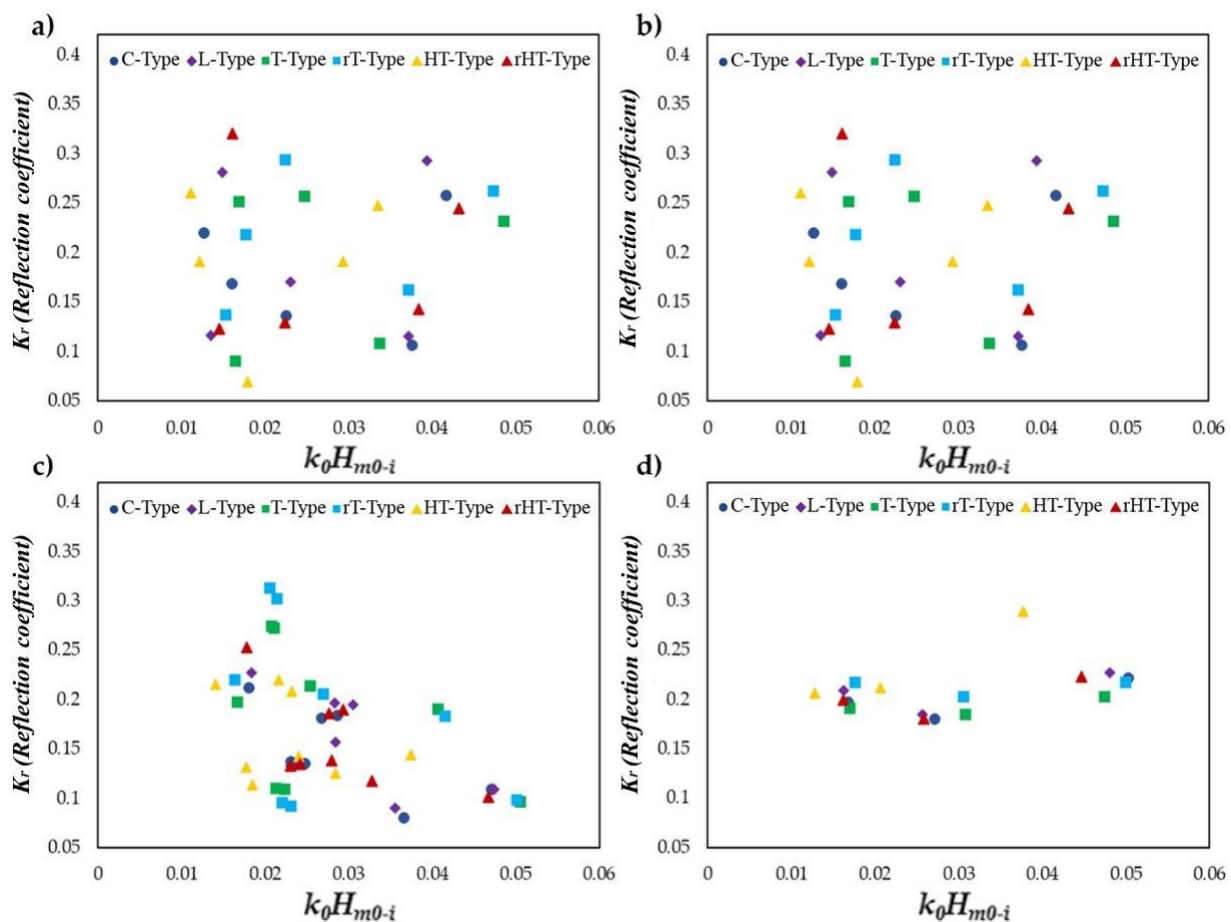

Figure 8. Reflection coefficient, K_r, versus incident wave steepness ($k_0 H_{m0\text{-}i}$) in different wave climates: (**a**) regular "poor" conditions; (**b**) regular "mild" wave conditions; (**c**) regular "extreme" wave conditions; (**d**) irregular "storm" wave conditions.

4.3. Wave Dissipation

The average dissipation coefficients are shown in Figure 6 (lower panel), while the detailed patterns of K_d versus the wave steepness are graphically represented in Figure 9. The most important aspect is that the presence of the head strongly influences the dissipation mechanisms, creating unfavorable conditions for the dissipation. This, in general, does not really look that great for two reasons: (1) lower dissipation is associated with a higher value of K_t or K_r, both having ruthless effects on wave protection and shipping, respectively; and (2) if you want to turn these barriers into wave-activated bodies for wave energy production (for instance, by inserting a power take-off at the basis of the stem), the only part available for power conversion is the one represented by the dissipation coefficient. A possible explanation for such behavior is that the heads act on the turbulence as a calming effect or by changing its structure (for instance, moving by a Kàrmàn vortex street to a tip vortex structure). Moreover, it seems confirmed that the bulk of turbulence occurs on the top of the stem, near the water surface, as expected.
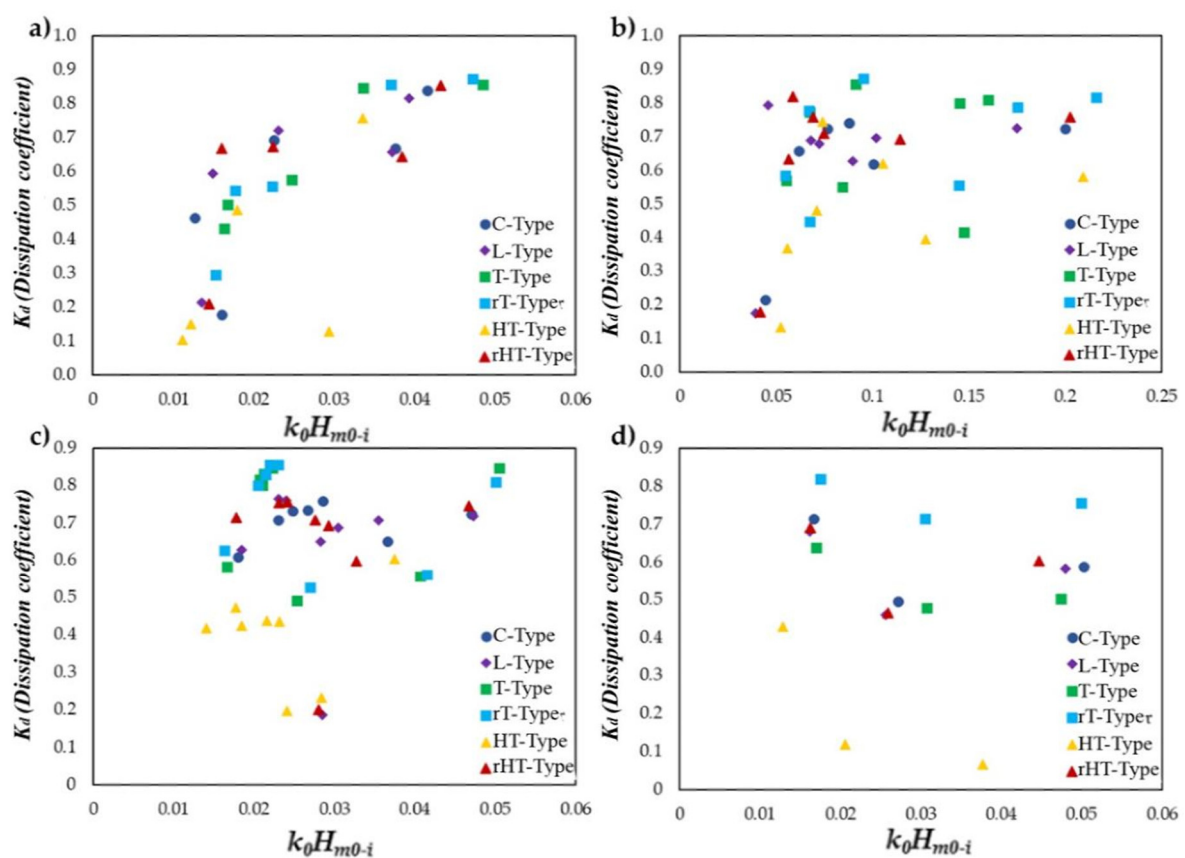

Figure 9. Dissipation coefficient, K_d, versus incident wave steepness ($k_0H_{m0\text{-}i}$) in different wave climates: (**a**) regular "poor" conditions; (**b**) regular "mild" wave conditions; (**c**) regular "extreme" wave conditions; (**d**) irregular "storm" wave conditions.

5. Discussion

5.1. Usefulness and Application of the Technology

This study reported laboratory tests on wave transmission for different bioinspired models. To better understand their performance, it can be noticed that rubble-mound breakwater with higher submergence tested by Hassanpour et al. [15], under similar wave conditions, showed average transmission coefficient values of 0.41 and 0.42 under regular and irregular wave regimes, respectively. The bioinspired model with the lowest transmission coefficient, the rT-Type, increases the average value of 0.65 for poor, mild, and extreme wave conditions, and 0.61 for storm sea states. These values are particularly

interesting, given that the experiments tested only a single row of bioinspired models. Finally, "volume efficiency" is evident when considering the large amount of rock that is required for the rubble-mound structures. The impact on the bottom is, in addition, totally different, as is the possibility to easily remove/upgrade the bioinspired defense system. For the cases where higher wave dissipations are required, bioinspired elements could be associated with other coastal protection systems, as suggested by Jordan and Fröhle [46]. In this vein, it is interesting to cite some existing examples of hybrid coastal defense systems in Australia, such as the pods used to shelter mangroves in Victoria [47], or rock fillets with mangroves in New South Wales [48,49]. Bioinspired solutions can also be applied to replace hard coastal defense systems, following the example of removing a seawall from San Diego Bay to plant marsh plants to reduce erosion [50].

In our case, one of the most promising solutions can be the integration with the beach drainage system [51], a technology proven to be effective, only if the bulk of incoming wave energy is absorbed (by a detached coastal defense system or something like this [52]). In addition, the proposed models could be associated with new beach improvements to reduce wave force and to extend the lifetime of such light interventions.

These approaches could represent a potential response to the growing demand to bridge the gap between coastal engineering and nature conservation [46], with the additional value of combining techniques having no adverse visual impacts.

5.2. Additional Hydrodynamic Considerations

The variation in wave transmission coefficients (K_t) for different wave conditions reported the diverse effect of the designed models, indicating a notable relation and interaction between the model shape and the wave type. The C-Type and "L-Type" models showed quite constant hydrodynamic behavior represented by comparable values of K_t for all the investigated wave conditions. Conversely, both configurations of the "T shape" (T-Type and rT-Type models) seem to better interfere with wave propagation, resulting in lower K_t values, which are inversely related to the energy content of incident waves. This effect is probably due to the specific shape that determines an increase in turbulence and loss of wave energy under mild and extreme wave conditions. This hydrodynamic behavior can be considered as a high performance and effective to create future permeable marine infrastructures. Indeed, a higher transmission in calm wave conditions, i.e., during summer, allows better permeability of the barrier, avoiding water stagnation and anoxia that negatively affect the local biodiversity and natural nearshore littoral transport. Conversely, the lower transmission in high-energy wave conditions determines a good action of the barrier in wave energy reduction and therefore in coastal protection. Nonetheless, the results obtained from the HT-Type and rHT-Type models are not fully clear. A heuristic explanation could address the hydrodynamic effect of the "head".

When a fluid flows around a body, forces act between the fluid and the surface due to viscosity. Among other phenomena, these intermolecular forces are mainly responsible for drag. However, as a result of the forces at play, the solid body's surface also endeavors to adhere the fluid to itself, inducing a no-slip condition where the fluid adheres to the surface. The layer above this adherent fluid layer cannot easily detach due to intermolecular attraction and pressure forces between the layers. Consequently, any flow around the body is tempted to conform to the surface profile. Provided that a body's shape features gradual transitions and the fluid's internal cohesion (viscosity) is sufficiently robust to counteract inertial forces, the flow can conform to the body's contour. A conventional hydrodynamic boundary layer forms around the body, with its thickness predominantly influenced by viscosity. When encountering sharp transitions or flowing around blunt bodies, the fluid frequently loses its ability to adhere to the profile. Subsequently, the boundary layer or flow starts to detach from the body's surface, a phenomenon known as boundary layer separation or flow separation. Following the separation point downstream, vortices commonly emerge, leading to turbulent flow. Since the flow no longer adheres to the body's surface beyond the separation point, the skin friction drag approaches zero. However, there

is a substantial decrease in pressure due to the dissipation of energy in the turbulent wake. This results in a significant rise in pressure drag, surpassing the reduction in skin friction drag by a considerable margin. Accordingly, in cases of flow separation, total parasitic drag (flow resistance) experiences a notable increase. Hence, the head present in HT-Type and rHT-Type models, evidently, acts as a turbulence-reducing factor.

As it is known, the flow regime is well predicted by the Reynolds number (*Re*), which is calculated using the following notable formula:

$$Re = \frac{VL}{\nu} \tag{4}$$

where *V* is the velocity, *L* represents the characteristic length, and ν is the kinematic viscosity of the fluid. In the present study, the maximum velocity at the surface was assumed for *V*, while *L* was equal to the wavelength at the toe of the models. With reference to "storm" random tests, we computed that $Re > 2 \times 10^5$, indicating turbulent flow patterns.

The calculation of the hydrodynamic penetration coefficient for the tested model is a complex issue. A simplified approach can be used to highlight a relationship between the shape of the models and their hydrodynamic resistance. The latter can be assumed as directly related to the transmission coefficient. Two geometrical characteristics were considered: the reference width for drag, ξ, and the reference thickness for drag, ε. In Figure 10, the geometrical features ξ and ε are indicated for each model. These two parameters arise with the processes dominated by dynamic drag (here intending both form drag and skin friction). ξ is representative of the frontal "impact" area; in the present study, the maximum width of the model was assumed (for models with a head, ξ represents the width of the "stem"). On the other hand, ε addresses the surface experiencing separated shear layers. Hence, ε coincides with: (i) about half the diameter for the C-Type model; (ii) the rear part of the C-Type model projected onto the axis parallel to the main wave direction; (iii) the contour starting at about the minimum thickness behind the frontal bulb and following the rest of the section for the T-Type and HT-type models; and (iv) the contour starting at the semi-circular leading edge and following the rest of the section for the rT-Type and rHT-Type models.
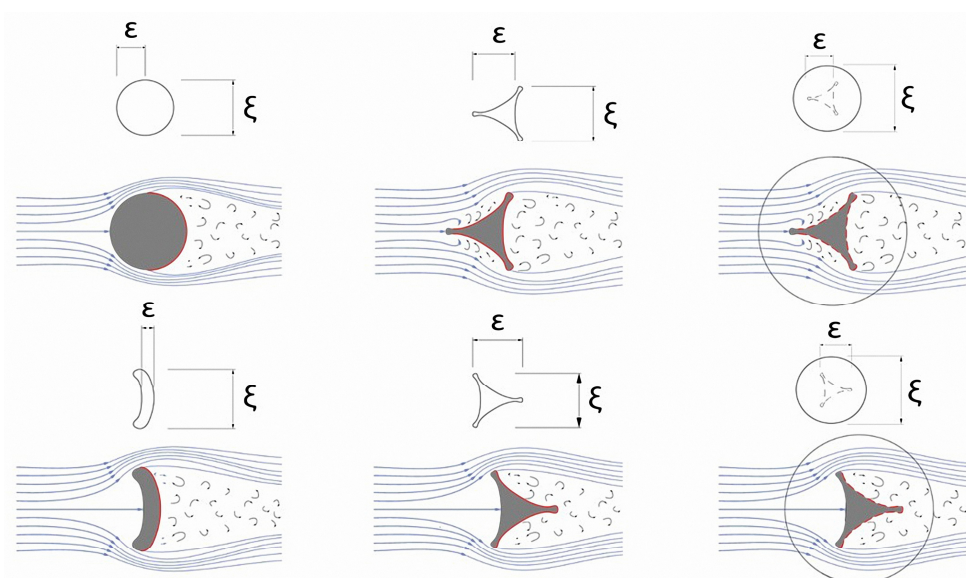

Figure 10. Identification of width, ξ, and thickness, ε, for the drag associated with the model shape and related hypothesized qualitative behavior of fluid flow.

The non-dimensional ration, ε/ξ, is plotted against the average of transmission coefficient in Figure 11. The points abide reasonably well to a potential law, whose coefficients

are evaluated fitting the data with the non-linear least squares method. The value of the correlation coefficient, R^2, is also indicated, providing confidence in the method.
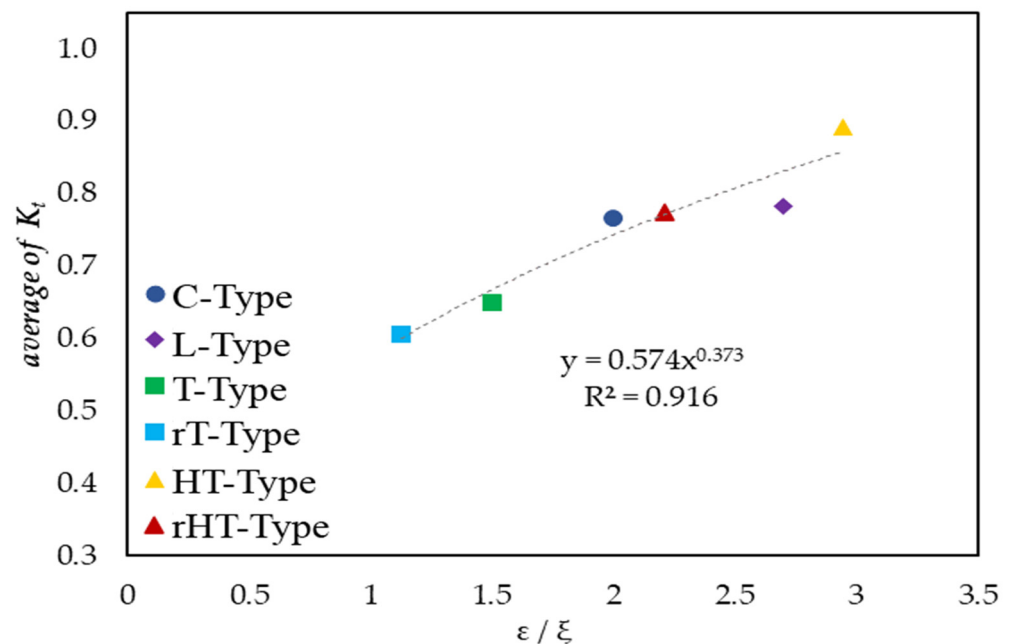

Figure 11. Average of transmission coefficient, K_t, versus the non-dimensional ratio between the reference width for drag, ξ, and the reference thickness for drag, ε.

6. Conclusions

The present article described the experimentation of simplified bioinspired models, evaluating their hydraulic performances and leading to interesting preliminary results. The variation in wave transmission and reflection and dissipation coefficients under different wave conditions revealed the diverse effects of the designed models. This indicates a notable relationship and interaction between the model shape and the wave type. Notably, the designed barriers demonstrated a significant hydraulic performance in wave attenuation. Compared to traditional barriers, these models occupy less space, enhancing water flow permeability and preventing anoxic effects on the shore. A tentative formula is provided to describe average values of K_t based on the geometrical features of models related to skin friction–drag processes. To improve the transmission performance, the bioinspired elements could be associated with other coastal protection measures, as suggested by Levy et al. [38]. For instance, the integration with the beach drainage system, a technology proven to be effective, only if the bulk of incoming wave energy is absorbed by a detached coastal defense, can represent a promising solution.

The achieved preliminary results are valuable for defining future shapes of coastal barriers at the macroscale. Subsequent form optimization and ultrastructural analysis can be conducted to develop a final bioinspired design that can be sustainably integrated into the local environment. This process requires an in-depth analysis of the local biotic and abiotic features, which should guide the structure, texture, and material composition of the future barrier. Using nature as model, measure, and mentor, the authors intend to promote a bioinspired approach for the fabrication of future coastal defense systems that do not impose themselves on nature, but, rather, are born from, inspired by, and integrated with it.

7. Patents

The setup used in this work refers to the Italian Patent Application "Multifunctional Bio Inspired System for Shoreline Protection and Energy Production". APPLICATION NUMBER: 102024000004192.

Institutional Review Board Statement: Not applicable.

Informed Consent Statement: Not applicable.

Data Availability Statement: The experimental data used in this study are available from the corresponding authors upon reasonable request.

Conflicts of Interest: The authors declare no conflicts of interest.

References

1. Core Writing Team; Lee, H.; Romero, J. (Eds.) *IPCC, 2023: Climate Change 2023: Synthesis Report. Contribution of Working Groups I, II and III to the Sixth Assessment Report of the Intergovernmental Panel on Climate Change*; IPCC: Geneva, Switzerland, 2023; pp. 35–115. [CrossRef]
2. Di Luccio, D.; Benassai, G.; Di Paola, G.; Rosskopf, C.M.; Mucerino, L.; Montella, R.; Contestabile, P. Monitoring and modelling coastal vulnerability and mitigation proposal for an archaeological site (Kaulonia, Southern Italy). *Sustainability* **2018**, *10*, 2017. [CrossRef]
3. Bridges, T.; Henn, R.; Komlos, S.; Scerno, D.; Wamsley, T.; White, K. *Coastal Risk Reduction and Resilience: Using the Full Array of Measures*; US Army Corps of Engineers Civil Works Directorate: Washington, DC, USA, 2013.
4. Unguendoli, S.; Biolchi, L.G.; Aguzzi, M.; Pillai, U.P.A.; Alessandri, J.; Valentini, A. A modeling application of integrated nature based solutions (NBS) for coastal erosion and flooding mitigation in the Emilia-Romagna coastline (Northeast Italy). *Sci. Total Environ.* **2023**, *867*, 161357. [CrossRef] [PubMed]
5. Haggi, A. Report on underwater excavation at the Phoenician Harbour, Atlit, Israel. *Int. J. Naut. Archaeol.* **2010**, *39*, 278–285. [CrossRef]
6. Franco, L. Ancient Mediterranean harbours: A heritage to preserve. *Ocean Coast. Manag.* **1996**, *30*, 115–151. [CrossRef]
7. ISOPE; Sharifahmadian, A. *Numerical Models for Submerged Breakwaters: Coastal Hydrodynamics and Morphodynamics*; Butterworth-Heinemann: Oxford, UK, 2015.
8. Hawkins, S.J.; Burcharth, H.F.; Zanuttigh, B.; Lamberti, A. *Environmental Design Guidelines for Low Crested Coastal Structures*; Elsevier: Amsterdam, The Netherlands, 2015.
9. Saengsupavanich, C.; Ariffin, E.H.; Yun, L.S.; Pereira, D.A. Environmental impact of submerged and emerged breakwaters. *Heliyon* **2022**, *8*, e12626. [CrossRef] [PubMed]
10. Perricone, V.; Mutalipassi, M.; Mele, A.; Buono, M.; Vicinanza, D.; Contestabile, P. Nature-based and bioinspired solutions for coastal protection: An overview among key ecosystems and a promising pathway for new functional and sustainable designs. *ICES J. Mar. Sci.* **2023**, *80*, 1218–1239. [CrossRef]
11. Browder, A.E.; Dean, R.G.; Chen, R. Performance of a submerged breakwater for shore protection. In *Coastal Engineering 1996*; ASCE Library: Reston, VA, USA, 1996; pp. 2312–2323.
12. THESEUS Project. Available online: https://cordis.europa.eu/project/id/672398 (accessed on 27 May 2024).
13. DELOS Project. Available online: https://cordis.europa.eu/project/id/EVK3-CT-2000-00041 (accessed on 27 May 2024).
14. Narayan, S.; Beck, M.W.; Reguero, B.G.; Losada, I.J.; Van Wesenbeeck, B.; Pontee, N.; Burks-Copes, K.A. The effectiveness, costs and coastal protection benefits of natural and nature-based defences. *PLoS ONE* **2016**, *11*, e0154735. [CrossRef] [PubMed]
15. Hassanpour, N.; Vicinanza, D.; Contestabile, P. Determining Wave Transmission over Rubble-Mound Breakwaters: Assessment of Existing Formulae through Benchmark Testing. *Water* **2023**, *15*, 1111. [CrossRef]
16. Postacchini, M.; Russo, A.; Carniel, S.; Brocchini, M. Assessing the hydro-morphodynamic response of a beach protected by detached, impermeable, submerged breakwaters: A numerical approach. *J. Coast. Res.* **2016**, *32*, 590–602.
17. Duarte Nemes, D.; Fabián Criado-Sudau, F.; Nicolás Gallo, M. Beach morphodynamic response to a submerged reef. *Water* **2019**, *11*, 340. [CrossRef]
18. Ranasinghe, R.; Turner, I.L. Shoreline response to submerged structures: A review. *Coast. Eng.* **2006**, *53*, 65–79. [CrossRef]
19. Hur, D.S.; Lee, W.D.; Cho, W.C. Three-dimensional flow characteristics around permeable submerged breakwaters with open inlet. *Ocean Eng.* **2012**, *44*, 100–116. [CrossRef]
20. Singhvi, A.; Luijendijk, A.P.; van Oudenhoven, A.P. The grey–green spectrum: A review of coastal protection interventions. *J. Environ. Manag.* **2022**, *311*, 114824. [CrossRef] [PubMed]

21. European Commission, Directorate-General for Research and Innovation. *Towards an EU Research and Innovation Policy Agenda for Nature-Based Solutions & Re-Naturing Cities: Final Report of the Horizon 2020 Expert Group on 'Nature-Based Solutions and Re-Naturing Cities': (Full Version)*; Publications Office: Luxembourg, 2015.

22. Schoonees, T.; Mancheño, A.G.; Scheres, B.; Bouma, T.J.; Silva, R.; Schlurmann, T.; Schüttrumpf, H. Hard structures for coastal protection, towards greener designs. *Estuaries Coasts* **2019**, *42*, 1709–1729. [CrossRef]

23. Moosavi, S. Ecological coastal protection: Pathways to living shorelines. *Procedia Eng.* **2017**, *196*, 930–938. [CrossRef]

24. Cohen-Shacham, E.; Walters, G.; Janzen, C.; Maginnis, S. Nature-based solutions to address global societal challenges. *IUCN Gland.* **2016**, *97*, 2016–2036.

25. Scheres, B.; Schüttrumpf, H. Nature-Based Solutions in Coastal Research–A New Challenge for Coastal Engineers? In Proceedings of the APAC 2019: 10th International Conference on Asian and Pacific Coasts, Hanoi, Vietnam, 25–28 September 2019; Springer: Singapore, 2019; pp. 1383–1389.

26. Seddon, N.; Chausson, A.; Berry, P.; Girardin, C.A.; Smith, A.; Turner, B. Understanding the value and limits of nature-based solutions to climate change and other global challenges. *Philos. Trans. R. Soc. B* **2020**, *375*, 20190120. [CrossRef] [PubMed]

27. Stachew, E.; Houette, T.; Gruber, P. Root Systems Research for Bioinspired Resilient Design: A Concept Framework for Foundation and Coastal Engineering. *Front. Robot. AI* **2021**, *8*, 109. [CrossRef] [PubMed]

28. Levy, N.; Berman, O.; Yuval, M.; Loya, Y.; Treibitz, T.; Tarazi, E.; Levy, O. Emerging 3D technologies for future reformation of coral reefs: Enhancing biodiversity using biomimetic structures based on designs by nature. *Sci. Total Environ.* **2022**, *830*, 154749. [CrossRef]

29. Reef Design Lab. Available online: https://www.reefdesignlab.com/ (accessed on 27 May 2024).

30. 3DPARE. Available online: https://www.giteco.unican.es/proyectos/3dpare/index.html (accessed on 27 May 2024).

31. Bulleri, F.; Chapman, M.G. The introduction of coastal infrastructure as a driver of change in marine environments. *J. Appl. Ecol.* **2010**, *47*, 26–35. [CrossRef]

32. McLachlan, A.; Defeo, O.; Short, A.D. Characterising sandy beaches into major types and states: Implications for ecologists and managers. *Estuar. Coast. Shelf Sci.* **2018**, *215*, 152–160. [CrossRef]

33. Barbier, E.B. Progress and challenges in valuing coastal and marine ecosystem services. *Rev. Environ. Econ. Policy* **2012**, *6*, 1–19. [CrossRef]

34. Ondiviela, B.; Losada, I.J.; Lara, J.L.; Maza, M.; Galván, C.; Bouma, T.J.; van Belzen, J. The role of seagrasses in coastal protection in a changing climate. *Coast. Eng.* **2014**, *87*, 158–168. [CrossRef]

35. Cavallaro, L.; Viviano, A.; Paratore, G.; Foti, E. Experiments on surface waves interacting with flexible aquatic vegetation. *Ocean Sci. J.* **2018**, *53*, 461–474. [CrossRef]

36. Stratigaki, V.; Manca, E.; Prinos, P.; Losada, I.J.; Lara, J.L.; Sclavo, M.; Sánchez-Arcilla, A. Large-scale experiments on wave propagation over Posidonia oceanica. *J. Hydraul. Res.* **2011**, *49* (Suppl. S1), 31–43. [CrossRef]

37. Larkum, A.W.; Orth, R.J.; Duarte, C.M.; Koch, E.W.; Ackerman, J.D.; Verduin, J.; Keulen, M.V. Fluid dynamics in seagrass ecology—From molecules to ecosystems. In *Seagrasses: Biology, Ecologyand Conservation*; Springer: Berlin/Heidelberg, Germany, 2006; pp. 193–225.

38. Fonseca, M.S.; Cahalan, J.A. A preliminary evaluation of wave attenuation by four species of seagrass. *Estuar. Coast. Shelf Sci.* **1992**, *35*, 565–576. [CrossRef]

39. Augustin, L.N.; Irish, J.L.; Lynett, P. Laboratory and numerical studies of wave damping by emergent and near-emergent wetland vegetation. *Coast. Eng.* **2009**, *56*, 332–340. [CrossRef]

40. John, B.M.; Shirlal, K.G.; Rao, S.; Rajasekaran, C. Effect of artificial seagrass on wave attenuation and wave run-up. *Int. J. Ocean. Clim. Syst.* **2016**, *7*, 14–19. [CrossRef]

41. Perrin, W.F.; Würsig, B.; Thewissen, J.G.M. (Eds.) *Encyclopedia of Marine Mammals*; Academic Press: Cambridge, MA, USA, 2009.

42. Jung, S. Swimming, flying, and diving behaviors from a unified 2D potential model. *Sci. Rep.* **2021**, *11*, 15984. [CrossRef]

43. Klopman, G.; Meer, J.W.V.D. Random wave measurements in front of reflective structures. *J. Waterw. Port Coast. Ocean. Eng.* **1999**, *125*, 39–45. [CrossRef]

44. Mansard, E.P.; Funke, E.R. The measurement of incident and reflected spectra using a least squares method. In Proceedings of the 17th International Conference on Coastal Engineering, Sydney, Australia, 23–28 March 1980; ASCE Library: Reston, VA, USA, 1980; pp. 154–172.

45. Guo, Y.C.; Mohapatra, S.C.; Soares, C.G. Wave energy dissipation of a submerged horizontal flexible porous membrane under oblique wave interaction. *Appl. Ocean Res.* **2020**, *94*, 101948. [CrossRef]

46. Jordan, P.; Fröhle, P. Bridging the gap between coastal engineering and nature conservation? A review of coastal ecosystems as nature-based solutions for coastal protection. *J. Coast. Conserv.* **2022**, *26*, 4. [CrossRef]

47. Morris, R.; Strain, E.M.; Konlechner, T.M.; Fest, B.J.; Kennedy, D.M.; Arndt, S.K.; Swearer, S.E. Developing a nature-based coastal defence strategy for Australia. *Aust. J. Civ. Eng.* **2019**, *17*, 167–176. [CrossRef]

48. Jenkins, C.; Russell, K. *Scott's Point Rock Fillets–Fish Friendly Erosion Mitigation*; NSW Department of Primary Industries: Bathurst, Australia, 2017.

49. Taylor, M. Options for Stabilising Riparian Estuarine Zones. In Proceedings of the NSW Coastal Conference, Port Stephens, Batemans Bay, Australia, 6–8 November 2017.

50. Davis, J.L.; Takacs, R.L.; Schnabel, R. Evaluating ecological impacts of living shorelines and shoreline habitat elements: An example from the upper western Chesapeake Bay. In *Management, Policy, Science, and Engineering of Nonstructural Erosion Control in the Chesapeake Bay*; 2006; p. 55. Available online: https://www.vims.edu/cbnerr/_docs/ctp_docs/ls_docs/06_LS_Full_Proceed.pdf#page=71 (accessed on 27 May 2024).
51. Damiani, L.; Petrillo, A.F.; Saponieri, A. Beach Dewatering Systems: Modelling coastal ground-water flow. In Proceedings of the 33RD IAHR Congress Water Engineering for a Sustainable Environment 2009, Vancouver, BC, Canada, 9–14 August 2009; pp. 7304–7311.
52. Ciavola, P.; Vicinanza, D.; Aristodemo, F.; Contestabile, P. Large-scale morphodynamic experiments on a beach drainage system. *J. Hydraul. Res.* **2011**, *49*, 523–528. [CrossRef]